Atmospheric Research 155 (2015) 73–86

Contents lists available at ScienceDirect

Atmospheric Research

journal homepage: www.elsevier.com/locate/atmos

Aircraft measurements of the vertical distribution and activation property of aerosol particles over the Loess Plateau in China

Junxia Li [a,b,*], Yan Yin [a,c,**], Peiren Li [b], Zhanqing Li [d,e], Runjun Li [d], Maureen Cribb [e], Zipeng Dong [d,f], Fang Zhang [d], Jin Li [g], Gang Ren [b], Lijun Jin [b], Yiyu Li [b]

[a] Key Laboratory for Aerosol–Cloud–Precipitation of China Meteorological Administration, School of Atmospheric Physics, Nanjing University of Information Science and Technology, Nanjing, Jiangsu 210044, China
[b] Weather Modification Office of Shanxi Province, Taiyuan, Shanxi 030032, China
[c] Collaborative Innovation Center on Forecast and Evaluation of Meteorological Disasters, Nanjing University of Information Science and Technology, Nanjing, Jiangsu 210044, China
[d] College of Global Change and Earth System Science, Beijing Normal University, Beijing 100875, China
[e] Department of Atmospheric and Oceanic Science and Earth System Science Interdisciplinary Center (ESSIC) University of Maryland, College Park, MD, USA
[f] Meteorological Institute of Shaanxi Province, Xi'an, Shaanxi 710017, China
[g] Meteorological Station in Anhui Province, Hefei, Anhui 230031, China

ARTICLE INFO

Article history:
Received 7 August 2014
Received in revised form 3 December 2014
Accepted 3 December 2014
Available online 10 December 2014

Keywords:
Vertical distribution
Size distribution
Activation property
Aircraft measurements
The Loess Plateau

ABSTRACT

For the first time, comprehensive aircraft measurements of atmospheric aerosols and cloud condensation nuclei (CCN) were made over the Loess Plateau in Shanxi, China. Data from six flights in July and August 2013 were analyzed. Fine aerosols were predominant over the region. On the one hazy day, the fraction of fine particles in the total aerosol load was the greatest. Aerosol number concentration decreased exponentially with altitude. Inversion layers caused low-level aerosol accumulation zones. The mean aerosol particle size increased with altitude, and the larger particles were mainly found above 2 km. Aerosol number size distributions at different height ranges showed two or three peaks. The aerosol number size distribution from 0.01 μm to 20 μm can be fitted with three log-normal distribution functions. The number concentration of CCN (N_{CCN}) decreased with altitude. N_{CCN} was linearly related to the CN concentration (N_{CN}). The fraction of CCN to CN ($f_{CCN/CN}$) at 0.3% SS was half of that at 0.4% SS. The $f_{CCN/CN}$ on the hazy day was lower than on the clear days. Vertical profiles of $f_{CCN/CN}$ and the effective diameter (ED) were similar, although the $f_{CCN/CN}$ increased with altitude.

1. Introduction

Increasing attention has been paid to aerosols because of their substantial influence on the atmospheric environment, clouds and precipitation, and the climate system. Atmospheric aerosols can serve as condensation nuclei for the formation of both cloud droplets and ice nuclei, and can change the microphysical properties of clouds, which in turn affects the formation of rain, snow, and other forms of precipitation (Hudson and Yum, 2001; Hudson et al., 2011; Tao et al., 2012; Lohmann and Feichter, 2005; Andreae and Rosenfeld, 2008). Changes in aerosol concentration can also affect cloud optical properties, cloud cover, and cloud lifetime (Haywood and Boucher, 2000). Many studies have been made to understand the physical, chemical, and optical properties of aerosol particles and their effects on cloud, precipitation and other weather phenomenon (e.g., Li et al., 2009, 2011a, 2011b, 2011c; Yin et al., 2000, 2002, 2010; Levin et al., 2005; Cui et al., 2006;

* Correspondence to: J. Li, Weather Modification Office of Shanxi Province, Taiyuan, China. Tel./fax: +86 351 7562202.
** Correspondence to: Y. Yin, Nanjing University of Information Science and Technology, Nanjing, Jiangsu 210044, China. Tel./fax: +86 25 58731207.
E-mail addresses: ljx22258@126.com (J. Li), yinyan@nuist.edu.cn (Y. Yin).

http://dx.doi.org/10.1016/j.atmosres.2014.12.004
0169-8095/

Grützun et al., 2008; Sabbah and Hasan, 2008; Kar et al., 2009; Xu et al., 2012; Fan et al., 2012; Salinas et al., 2013; Calvo et al., 2013; Zhao et al., 2015). However, large uncertainties still remain in the study of the aerosol particles especially the vertical distributions of aerosols in the lower troposphere (Stettler and von Hoyningen-Huene, 1996; Terry, 2008). The vertical distributions of aerosols such as the number concentration (N_a) and effective diameter (ED) have strong effects on estimates of direct and indirect radiative forcing by aerosols (IPCC, 2007). The observed aerosol properties such as vertical profiles of N_a and ED vary with time, location, and atmospheric conditions (Welton et al., 2002; Han et al., 2003; O'Connor et al., 2008; Campbell et al., 2013; Li et al., 2013; Ma and Yu, 2014; Wang et al., 2014). Therefore, there is a need to better understand aerosol vertical distributions.

To understand the impact of aerosols on clouds, it is crucial to find relationships between aerosols and cloud condensation nuclei (CCN). Aerosol particles that act as CCN and their interactions with cloud droplets are the key uncertainties for determining effects of aerosols on climate. Formation of cloud droplets is not only influenced by aerosol number concentrations, but also by their size distribution and chemical composition. Cloud microphysics also depends on dynamic and thermodynamic conditions, mainly updraft and cloud supersaturation. Therefore, another difficulty encountered in aerosol research is the relationship between aerosol particles and cloud droplets. Researches including observations near the ground and many extensive aircraft measurements have focused on the activation properties of aerosols and CCN (Junge and McLaren, 1971; Fitzgerald, 1973; Hudson and Yum, 2001; Yum and Hudson, 2002, 2004; Frank et al., 2006; Dusek et al., 2006; Hudson and Mishra, 2007; Kuwata et al., 2008; Hudson et al., 2009, 2010, 2012; Hudson and Noble, 2009, 2014a, 2014b; Deng et al., 2011, 2013).

More direct and long-term observations are needed to characterize height-resolved aerosol properties and to provide essential validation for modeling and satellite remote sensing. While ground-based remote sensing of the vertical profiles of aerosol and CCN (e.g., Gras, 1995; DeFelice and Saxena, 1994; DeFelice, 1996; Ghan and Collins, 2004; Ghan et al., 2006; Liu et al., 2011, 2012) has been attempted, aircraft provides direct in situ atmospheric measurements (Anderson et al., 2003; Haywood et al., 2003; Zhang et al., 2006). Johnson et al. (2000) studied the evolution of aerosols, clouds, and boundary-layer characteristics using C-130 aircraft observations collected during the first ACE-2 Lagrangian experiment, and suggested that the important processes controlling the concentration of Aitken mode particles included diffusional scavenging of interstitial aerosols by cloud droplets and similarly enhanced coagulation of Aitken mode and accumulation mode particles. Snider et al. (2000) also analyzed data from the ACE-2 and reported the effect of relative humidity (RH) on aerosol particle size distributions.

Cloud residue and interstitial aerosols from non-precipitating clouds observed by aircraft over an industrial urban area in northern China and chemical properties of haze particles over a coal-burning region on the Loess Plateau in winter were investigated by Li et al. (2011a, 2011b, 2011c, 2012). Using aircraft optical spectrometer probes, fine-mode and coarse-mode aerosol size distributions were recorded within and above the planetary boundary layer (PBL) in the vicinity of Beijing (Zhang et al., 2006, 2009). That analysis suggested that fine aerosol particles were dominant within the PBL with number concentrations of 5000 cm^{-3} and mode diameter 0.3 μm. Dust particles dominated above the PBL with number concentrations of 2.5 cm^{-3} and diameters of 2.5 μm. Liu et al. (2009) used an airborne optical spectrometer probe to generate 152 vertical profiles of N_a and size distributions over Beijing. The average surface-level number concentration was ~6600 cm^{-3}. Because of the strict control of airspace and high operating costs, there is a lack of aircraft observations of N_a and size distributions in the lower troposphere over both urban and rural areas. Also, most of the current flight-based research is focused on detecting accumulation-mode aerosol particles (0.1–3 μm) using an optical spectrometer probe. Concurrent aircraft measurements of aerosol particles in the 0.01–20 μm range and CCN are rare.

During the International Aerosol-CCN-Cloud Closure Experiment (ACCCExp13), which is an integral part of the East Asian Study of Tropospheric Aerosol and Impact on Regional Climate (EAST-AIRC) (Li et al., 2011a, 2011b, 2011c), an airborne campaign was conducted in July 2013 in Shanxi Province on the Loess Plateau of China. Comprehensive observations of atmospheric aerosol characteristics in this region were collected for the first time. In this paper, data from six flights on non-precipitating days were selected to analyze the spatial distribution of aerosol properties during the summer. One flight was made under hazy condition and the other flights were made on clear-sky days or clear sky with small amount of light cumulus.

Section 2 describes the sites and the air campaign. The vertical and particle spectral distribution characteristics of aerosols in different modes, as well as the influence of the temperature inversion layer (TIL) structure on the aerosol distribution are presented in Section 3. Results and discussion from experiments involving aerosol activation properties and the relationship between aerosols and CCN are also presented in this section. A conclusion follows in Section 4.

2. Description of the field campaign

2.1. Observation area

Shanxi Province is located in northern China, east of the Yellow River and west of the Taihang Mountains (Fig. 1). The Loess Plateau covers most of the province, and the average surface elevation of the entire province is 1000 m. Shanxi is situated in the temperate continental monsoon climate zone, and average annual precipitation ranges from 400 to 650 mm. This is an important energy and industrial chemical center of China. In conjunction with rapid economic growth in the region, the increase in industrial emissions of anthropogenic aerosol particles may have had a strong impact on regional air quality and climate. This has garnered much public interest in recent years. Three surface aerosol observatories were established on the Loess Plateau: Taiyuan (112.55° E, 37.867° N, elevation 778 m above sea level, or ASL), Wenshui (112.14° E, 37.26° N, elevation 800 m, ASL), and Xinzhou (112.70° E, 38.73° N, elevation 800 m, ASL). Their locations are shown in Fig. 1. Flight observations were mainly done near these three sites.

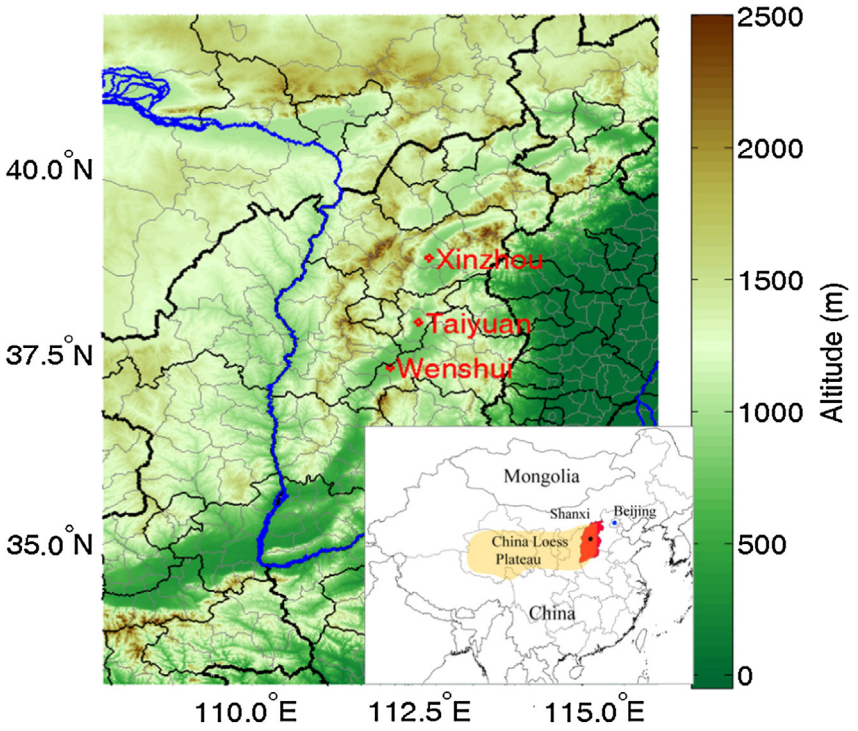

Fig. 1. The area over which flights were made and locations of the three surface aerosol observatories (Taiyuan, Wenshui, and Xinzhou). The inset map shows the location of the observation area in China. The yellow and red shaded areas show the China Loess Plateau and Shanxi Province, respectively. Altitude is height above sea level (ASL).

2.2. Measurements and datasets

A Y-12 turboprop airplane previously used for weather modification research was converted into an aerosol observation platform. The typical aircraft speed was 60–70 ms^{-1}, rate of ascent and descent was 2–5 m s^{-1}. It was equipped with multiple aerosol measurements that cannot be obtained by single instruments period. Each instrument was calibrated and tested rigorously during a ground-based campaign prior to the airborne campaign to maximize instrument performance. A passive cavity aerosol spectrometer probe (PCASP-100X, DMT, USA) was used to observe aerosol particles with diameters 0.1–3.0 μm within 30 variable size bins at a frequency of 1 Hz, and the time resolution is 1 second. The PCASP was calibrated by using polystyrene latex spheres (PSL) of Particle Metrics Inc. (PMI) every year before the measurements took place. Aerosol particles with diameters 10–487 nm were recorded by a scanning mobility particle sizer (SMPS, Model 3034, TSI, USA) in 54 bins. The SMPS can automatically correct the observations according to ambient pressure and temperature. Aerosol particles with diameters 0.5–20 μm were measured by an aerodynamic particle sizer (APS, Model 3321, TSI, USA) in 52 bins. The smallest measurable particle concentration is 0.001 cm^{-3}; this instrument can correct for pressures between 400 and 1030 mbar automatically. Both of the time resolutions of SMPS and APS were set to 4 minutes. CCN was recorded by a continuous-flow dual cloud condensation nuclei counter (CCN_C–200, DMT, USA) in 20 bins period. This has two cloud chambers that can be set to scan over two different supersaturation ranges simultaneously. The time resolution of CCN_C–200 is 1 second. The CCN_C–200 was calibrated with ammonium sulfate particles (Rose et al., 2008) before the observation campaign period. This included calibration of air flow, supersaturation ratio, temperature and pressure. During the flights, a CCN inlet pressure controller (CIPC, DMT, USA) was equipped with the CCN_C–200 corrected the pressure influences. Two sample inlets on the top of the airplane designed to minimize aerosol loses. These inlets connect to the measurements as directly as possible to avoid turns or corners to the best extent. SMPS and CCN_C–200 shared one inlet through a tee shunt and a diffusion dryer is connected before the sample goes into the SMPS period. The APS uses the other inlet. Meteorological parameters such as ambient temperature (T) and relative humidity (RH) were also measured by other onboard equipment during flights. Real-time locations such as longitude, latitude, and altitude were recorded by a Global Positioning System (GPS) device. Note that data in the first bins of SMPS (0.01 μm), PCASP (0.09–0.1 μm) and APS (0.523 μm) are inaccurate due to detection limits, so they are eliminated from analysis.

Aerosols are usually divided into groups, or modes according to particle size (Whitby, 1978). Given that aerosol measurements were obtained with different instruments, particle size mode ranges were divided for consistency of all instruments. In this study, SMPS data from bins 2 to 34 (11–110 nm) were used to study nucleation mode aerosols, PCASP data from bins 2 to 30 (0.11–3 μm) were used to study accumulation mode aerosols, and APS data from bins 26 to 52 (3–20 μm) were used to study coarse mode particles. All times are in China Standard Time (CST), and during the days of these

flights, sunrise was at about 0600 CST, local noon was near 1200 CST, and sunset occurred at 1900 CST. Altitudes are distances above sea level (ASL).

Data from six flights were selected for the study. The dates of the flights are 31 July 2013 (cloudless and hazy), and 1–5 August 2013 (clear-sky). The plane was based at Taiyuan Wusu International Airport and flew from there to Wenshui and Xinzhou. Flight segments started at a specific altitude and proceeded in downward spirals. Measurements were obtained over 5-minute periods at 300-m altitude intervals. Flight details are given in Table 1 and flight tracks are shown in Fig. 2.

3. Results and discussion

3.1. Statistical characteristics of the number concentration of aerosol particles (N_a)

The highest number concentrations of aerosols (N_a) in nucleation and accumulation modes occurred on 31 July, which was a hazy day over the Taiyuan and Wenshui sites. The maximum 4-minute nucleation mode concentration reached 42,689 cm^{-3} with an average of 8334 cm^{-3} over the 3.5-hour flight. The maximum 1-second value of the accumulation mode aerosol concentration was 5436 cm^{-3} with an average value over the 3.5-hour flight of 1317 cm^{-3}. The high concentration of these fine particles led to low visibility on this day. On 1 August, aerosol concentrations were lower over the flight domain (Taiyuan and Xinzhou). During the measurement period (1738–1937 CST), the maximum 4-minute value of the nucleation mode aerosol concentration was 19,722 cm^{-3} with an average value of 3178 cm^{-3} over the 2-hour flight, and the maximum and minimum 1-second concentrations of accumulation mode aerosol concentration were 5650 cm^{-3} and 326 cm^{-3} with the average value of 1022 cm^{-3} during the 2-hour flight. A rain shower that occurred at 1400 CST was responsible for some aerosol washout. From 2 to 4 August, flights were concentrated over Taiyuan and Wenshui. On 2 August, a few shallow cumulus clouds were present. The sky was cloudless on 3 and 4 August. The peak 4-minute nucleation mode aerosol concentration (10,004 cm^{-3}) was lower on 2 August, and the mean number concentration was 2.0 $\times$ 10^3 cm^{-3} over the 2-hour flight, this was probably influenced by processes occurring in the clouds observed during this flight. On 3–4 August, nucleation mode particle concentrations were significantly greater than accumulation mode aerosol concentrations. The observation area moved to Xinzhou on 5 August. Nucleation mode aerosol particle concentrations were the lowest on this day; maximum (4-minute) and mean (over 2-hour flight) aerosol concentrations were 3653 cm^{-3} and 1258 cm^{-3}, respectively. Maximum 1-second concentration of accumulation mode aerosol was 3782 cm^{-3}, and mean concentration over the 2-hour flight was 1256 cm^{-3}, respectively. From 31 July to 5 August, the weather was showery in Xinzhou. This resulted in low fine particle concentrations over that site.

In summary, nucleation and accumulation mode aerosol particles dominated over the study area during the field campaign. The mean magnitude of concentration of these particles was 10^3 cm^{-3}, and the maximum magnitude of N_a reached 10^4 cm^{-3}. Coarse mode particles were very few, and the mean magnitude of concentration of coarse mode particles was 1 cm^{-3}. Thus, we mainly focus on nucleation and accumulation mode aerosol particles in this article. Table 2 summarizes N_a for three modes measured during each flight.

3.2. Vertical profiles of T and RH

Previous aircraft observational studies have shown that aerosol vertical profiles have a close relationship with PBL structure (e.g., Johnson et al., 2000; Zhang et al., 2006). The vertical profile of N_a is relatively uniform within the PBL, indicating that it is well-mixed period. Concentrations decrease sharply with distance above the PBL. The structure of the PBL is crucial, it affects the shape of vertical profiles of N_a and the vertical profile of size distribution in the lower troposphere (Johnson et al., 2000; Zhang et al., 2006; Han et al., 2008). Fig. 3 shows mean vertical profiles of T and RH during each flight. A moist and shallow surface mixed layer (SML) extended from the surface (778 m ASL) to about 500 m above the surface each day. Within the SML, temperature decreased with altitude, and the RH was high. The SML was also capped by a shallow and stable temperature inversion layer (TIL) on most days (31 July and 2–4 August). A second TIL was observed between 2200–2500 m on 31 July. A thicker TIL capped the SML on 3 August and 4 August. A second TIL was also observed on these days, extending from 2400 to 3000 m and from 2000 to 2300 m, respectively. On 1 August and 2 August, a shallow TIL was seen above 2000 m.

3.3. Vertical profile of particle number concentration (N_a)

Fig. 4 shows mean vertical profiles of N_a for the three aerosol modes from all flights. All instruments onboard the aircraft were turned on and started taking measurements before take-off. N_a generally increases from the surface to 1200 m, then decreases sharply with altitude. The first peak in N_a appears between 1000 and 1400 m. For example, for accumulation mode particles (Fig. 4b), from 31 July to 5 August,

Table 1
Flight summary.

Date	Time range (CST)	Weather condition	Domain covered	Altitude ASL (m)
2013-07-31	10:32–13:48	Cloudless, haze	Taiyuan, Wenshui (111.8–112.7° E, 37.3–38.0° N)	778–3800
2013-08-01	17:29–19:37	Small amount of light cumulus	Taiyuan, Xinzhou (112.4–113.0° E, 37.5–39.0° N)	778–5200
2013-08-02	15:04–16:31	Small amount of light cumulus	Taiyuan, Wenshui (111.8–112.7° E, 37.0–38.0° N)	778–4900
2013-08-03	09:51–11:44	Clear, cloudless	Taiyuan, Wenshui (111.8–112.8° E, 37.3–37.8° N)	778–4425
2013-08-04	10:57–12:31	Clear, cloudless	Taiyuan, Wenshui (111.8–112.8° E, 37.3–38.0° N)	778–3780
2013-08-05	15:18–17:06	Small amount of light cumulus	Taiyuan, Xinzhou (112.2–112.9° E, 37.6–39.0° N)	778–3820

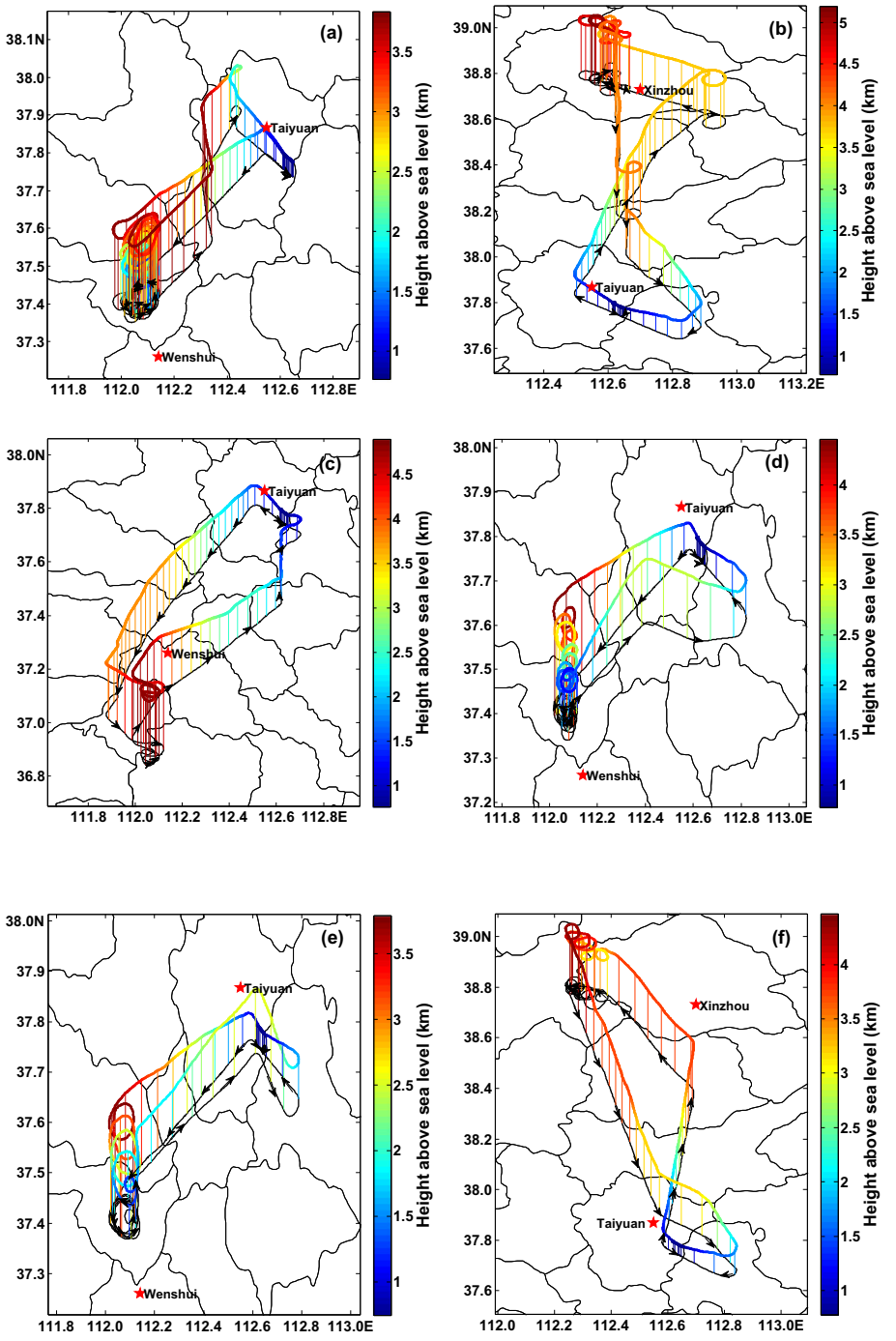

Fig. 2. Flight tracks made on (a) 31 July 2013, (b) 1 August 2013, (c) 2 August 2013, (d) 3 August 2013, (e) 4 August 2013, and (f) 5 August 2013. The color bar shows the height above sea level (ASL) in km. Stars show the locations of the three surface aerosol observatories.

maxima in N_a measured during each successive flight are 5436 cm^{-3} near the 1000-m level, 5650 cm^{-3} at the 1081-m level, 4914 cm^{-3} at the 1296-m level, 3493 cm^{-3} at the 1010-m, 5630 cm^{-3} at the 1084-m level, and 3782 cm^{-3} at the 800-m level, respectively. Smaller secondary peaks above 2000 m appear in most of the vertical profiles of N_a. N_a values for nucleation mode aerosols are at least one order of magnitude larger than N_a values of accumulation mode aerosols near the surface (Fig. 4a and b). N_a for coarse mode aerosols is low at all altitudes (<1 cm^{-3}) and shows no obvious trend with altitude (Fig. 4c).

Aerosols accumulated in a zone at the bottom of the TIL. Maxima in aerosol number concentration were observed in this layer. Flight records show that aerosols also accumulated in a

Table 2
Statistics describing N_a for three modes. (N_a: cm^{-3}). Time resolution of the "Max." and "Min." value of nucleation mode and coarse mode aerosols was 4-minute, time resolution of "Max." and "Min." of accumulation mode aerosols was 1-second, and the "Ave." was the flight-time (2–3.5 hours) averages.

Date	Nucleation mode (0.01–0.11 μm)			Accumulation mode (0.11–3 μm)			Coarse mode (3–20 μm)		
	Max.	Min.	Ave.	Max.	Min.	Ave.	Max.	Min.	Ave.
2013-07-31	42,689	559	8334	5436	172	1317	0.88	0	0.1
2013-08-01	197,22	521	3178	5650	326	1022	n/a	n/a	n/a
2013-08-02	10,004	270	2053	4914	381	1301	1.56	0.1	0.52
2013-08-03	28,817	89	2844	3493	198	830	1.27	0.3	0.7
2013-08-04	20,012	150	4485	5630	523	1337	1.45	0.24	0.48
2013-08-05	3653	253	1258	3782	324	1256	0.92	0.31	0.52

n/a: Not available.

hazy layer from 2000 to 3200 m. This may be because there was another TIL at a higher altitude. These measurements indicate that N_a profiles are different under different weather conditions.

Exponential fits to the mean vertical profiles of nucleation mode and accumulation mode N_a are shown in Fig. 4a and b. For the full profile (red dashed line), the following fitting equation (Eq. (1)) was used:

$$N_a = N_{surface} e^{\left(-(H-H_{surface})/H_p\right)} \quad (1)$$

where $N_{surface}$ is the surface-level particle number concentration, H_p is the scale height particle distribution in the vertical direction, and $H_{surface}$ is the local surface altitude above sea level (Seinfeld and Pandis, 1997; Fernández-Gálvez et al., 2013; Liu et al., 2009). Parameters describing the exponential fits are given in Table 3. The relatively high values of $N_{surface}$ indicate that aerosol number concentrations are generally high in the central region of the Loess Plateau on non-precipitation days in summer.

3.4. Vertical profile of particle effective diameter (ED)

ED is another important parameter describing the size of aerosol particles. It is defined as the ratio of the third to the second moment of the aerosol number size distribution (Eq. (2)), i.e.,

$$ED = \frac{\sum_{D_i} {D_i}^3 N(D_i)}{\sum_{D_i} {D_i}^2 N(D_i)} \quad (2)$$

where D_i represents the mean geometric diameter in the ith bin and $N(D_i)$ represents the number concentration in the ith bin.

Fig. 5 shows vertical profiles of ED for three aerosol modes from all flights. In general, ED increases with altitude. The largest ED was measured between 2000 and 3500 m and above 3500 m. Most ED of nucleation mode aerosols is less than 0.09 μm and the majority of ED of accumulation mode aerosols are less than 0.8 μm. Similar results were found by Liu et al. (2009) who reported that over Beijing, mean aerosol effective radii increased slightly with altitude and were less than 0.4 μm. Snider et al. (2000) showed that RH has an effect on aerosol size distributions. Although high RH values are seen above 3000 m and most of the larger aerosol particles are measured above 2000 m, no strict correlation between RH and aerosol size is seen. The ED represents the mean size of particles, so particles with different ED generally come from different sources. The combination of information from ED vertical profiles and N_a vertical distributions suggests that the majority of aerosols within the PBL are fine particles with ED less than 0.5 μm. These particles may originate via gas-to-particle formation involving local or regional pollutant emissions. Particles with ED greater than 0.5 μm are distributed at higher altitudes, suggesting that these particles were transported to the region from afar.

3.5. Vertical variation of aerosol number size distribution

Atmospheric aerosols are composed of different chemical compounds and a variety particle sizes. The distribution of aerosol number concentration with particle size, known as the aerosol average spectral distribution, is an important physical quantity used to describe the aerosol number size distribution. Aerosols in different areas and in different atmospheric environments have different spectral distributions. Changes in atmospheric conditions will change a particle's hygroscopic properties, as will condensation and collision processes, leading to a change in aerosol spectrum. Aerosol average spectral distributions at the following altitude ranges were analyzed: 778–1000 m, 1000–2000 m, 2000–3000 m, 3000–4000 m, and 4000–5000 m. A multi-lognormal distribution function (Eq. (3)) was used to fit the measured aerosol number size distributions within each altitude range:

$$\frac{dN(D)}{d\mathrm{Log}\left(D_p\right)} = \sum_{i=1}^{n} \frac{N_i}{\sqrt{2\pi}\log\left(\sigma_{g,i}\right)} \exp\left[-\frac{\left(\log(D_p)-\log\left(D_{g,i}\right)\right)^2}{2\left(\log\sigma_{g,i}\right)^2}\right] \quad (3)$$

where n is the number of modes per size distribution for the best fit, D_p is the peak aerosol diameter, N_i is the aerosol number in mode i, $D_{g,i}$ is the geometric mean diameter of the mode i, and $\sigma_{g,i}$ is the standard deviation of mode i (Seinfeld and Pandis, 1997; Sun et al., 2013). Fig. 6 shows the average spectral distribution of aerosols within different altitude ranges, and the lognormal fits to the aerosol spectrum. Parameters that characterize the number size distributions of the three aerosol modes in different altitude zones are listed in Table 4.

From the surface to 1000 m, three peaks in aerosol number concentration appear at 0.05 μm, 0.12 μm and 1.45 μm for the nucleation, accumulation and coarse modes, respectively. A

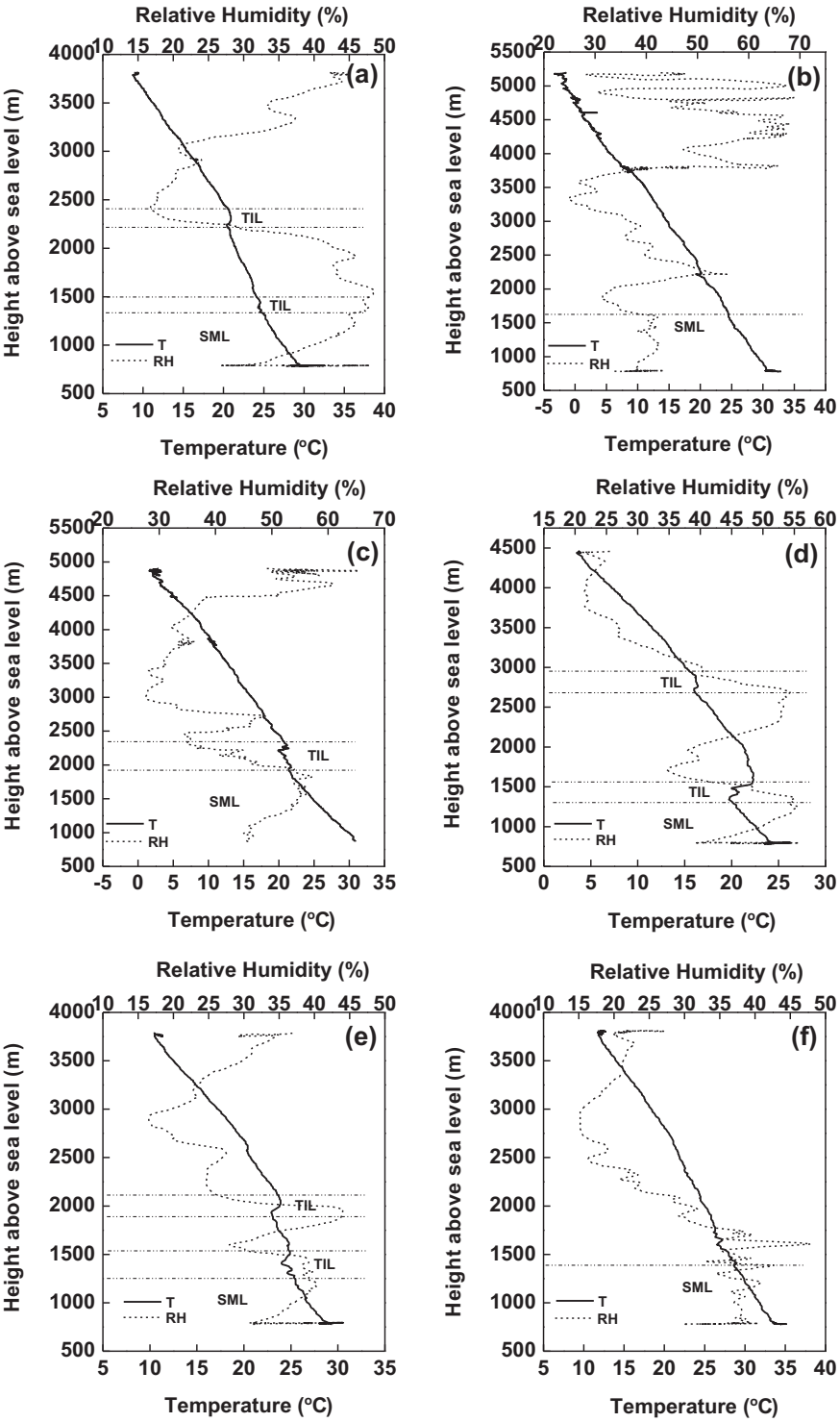

Fig. 3. Vertical profiles of temperature (solid lines) and relative humidity (dashed lines) measured on (a) 31 July 2013, (b) 1 August 2013, (c) 2 August 2013, (d) 3 August 2013, (e) 4 August 2013, and (f) 5 August 2013. The acronym "SML" stands for "surface mixed layer" and the "TIL" stands for "temperature inversion layer.".

bi-modal distribution best describes the aerosol spectrum in this layer (Fig. 6a). From 1000 m to 2000 m, aerosols with ED less than 2 μm contribute the most to the large aerosol number concentration. Peaks in aerosol number concentration appear at 0.065 μm, 0.19 μm, and 2.3 μm for the nucleation, accumulation, and coarse modes, respectively (Fig. 6b). The aerosol concentration is significantly reduced between 2000 m and 3000 m. A bi-modal size distribution is also seen within this

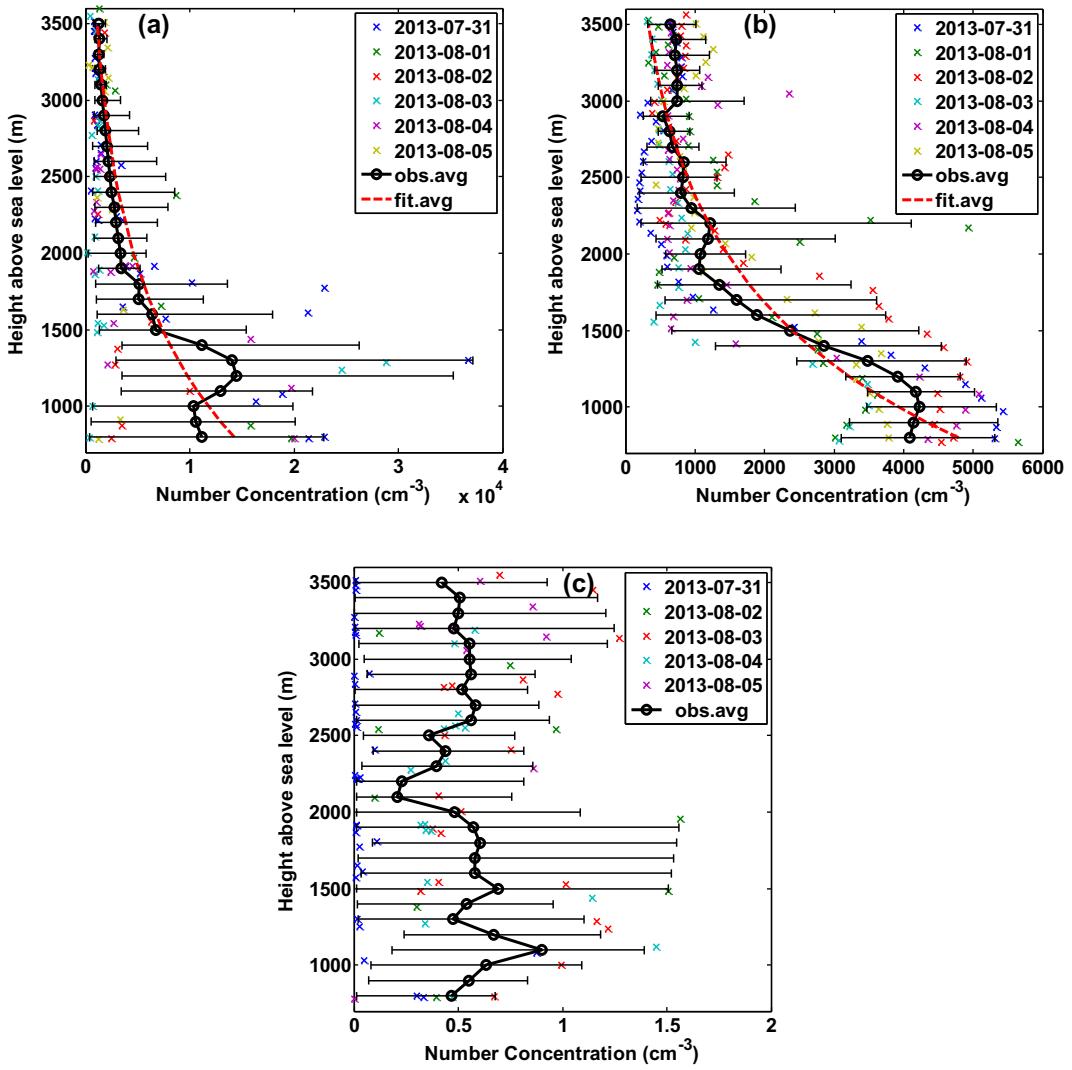

Fig. 4. Vertical profiles of mean number concentration from all flights (solid black line with hollow circles) for (a) nucleation, (b) accumulation and (c) coarse mode aerosol particles. Observations are plotted as colored x where the color represents the flight date. Horizontal black lines show the range of values (minimum and maximum values) observed at each altitude. The dashed red line represents the regression curve described by Eq. (1) (fitted to data from the surface upwards).

altitude range. Peaks of three modes in aerosol number concentration appeared at 0.08 μm, 0.2 μm, and 2.05 μm (Fig. 6c). The aerosol spectrum is similar in the 3000–4000 m altitude range, but peaks in aerosol number concentration are sharply reduced for particle sizes greater than 0.2 μm, and a tri-modal distribution is seen (Fig. 6d). The aerosol spectrum above 4000 m also shows a clear tri-modal distribution. Peak concentration order is no more than 10^3 cm^{-3} (Fig. 6e).

In general, the total N_a of each mode decreased with altitude. A sharp decrease in the N_a is seen in the aerosol size distribution at 0.2 μm. The magnitude of the N_a is less than 10^3 cm^{-3} when the ED is greater than 0.2 μm. From the surface to 5000 m, the width of the aerosol size distribution narrows in Mode I and Mode II, but broadens slightly in Mode III. According to the three modal lognormal distribution fits (solid colored curves in Fig. 6), nucleation mode aerosols (Mode I) and accumulation mode aerosols (Mode II) contribute the most to the total aerosol number concentration. Aerosol number size distributions in different altitude ranges are nearly the same, with most of the distributions showing two or three peaks.

Table 3
Parameters describing the exponential fits given in Eq. (1).

Fitting equation	$N_a = N_{surface} e^{(-(H-H_{surface})/H_p)}$		
Parameters	$N_{surface}$	$H_{surface}$	H_p
Accumulation mode	4891.7	778	1011
Nucleation mode	14,541	778	1064

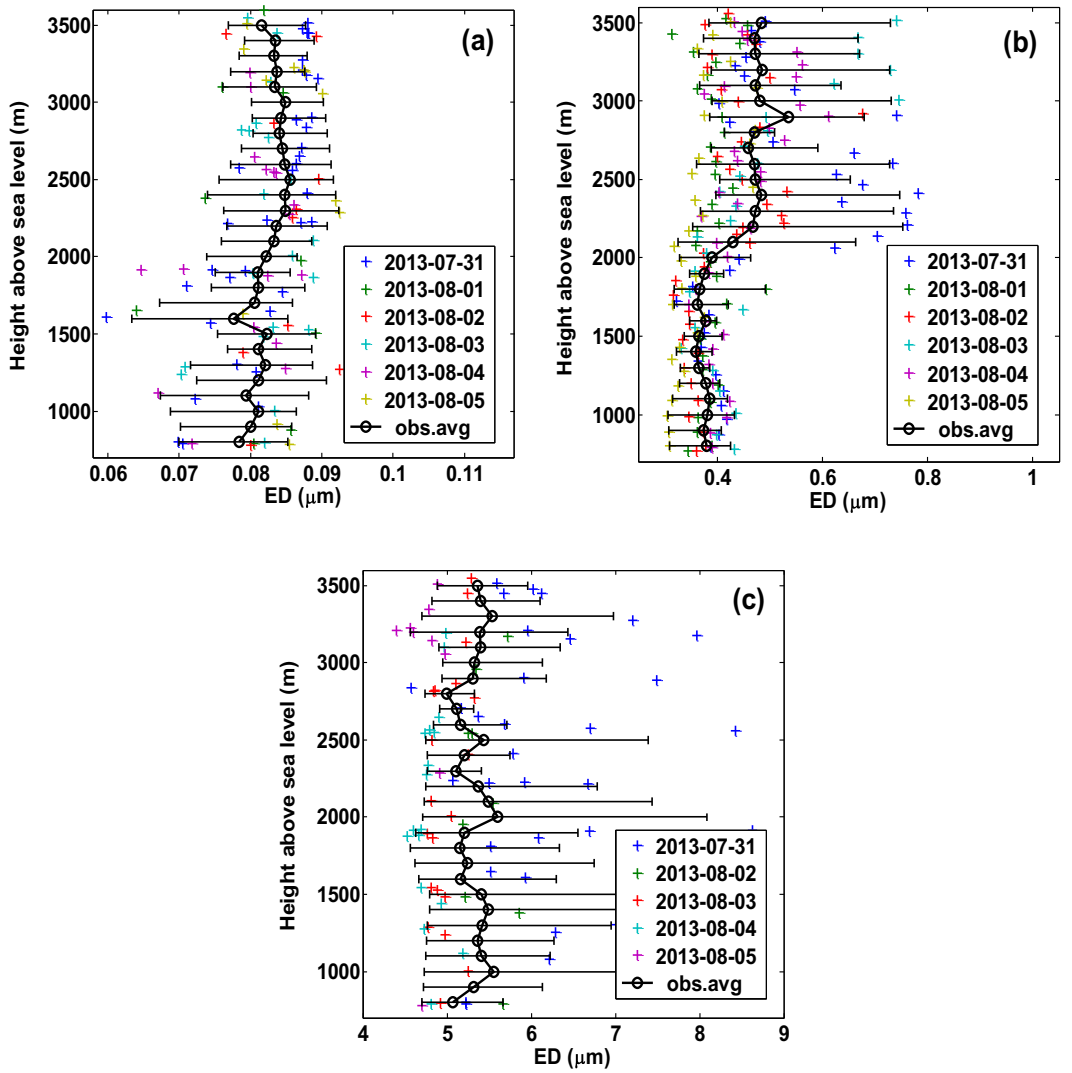

Fig. 5. Vertical profiles of mean effective diameters (ED) from all flights for (a) nucleation, (b) accumulation and (c) coarse mode aerosol particles. The caption is the same as Fig. 4.

3.6. Vertical properties of CCN and $f_{CCN/CN}$

3.6.1. Vertical distributions of N_{CCN}

CCN are the key link between aerosols and cloud droplet formation. CCN concentration and its relationships with aerosols were studied by selecting CCN and condensation nuclei (CN) data from the CCN_C-200 and the SMPS, respectively. Fig. 7 shows the vertical profiles of N_{CCN} with altitude at 0.3% and 0.4% supersaturation (SS) measured during the flights. Distributions of N_{CCN} at these two SS are consistent. Both distributions decrease with altitude.

N_{CCN} as a function of CN concentration (N_{CN}) at two SS (0.3% and 0.4%) is shown in Fig. 8. Data are from all flights. Linear regressions were made. Correlation of determination (R^2) of the linear regressions is 0.984 when SS is 0.3% and 0.995 when SS is 0.4%. This suggests that a linear fit is very suitable between N_{CN} and N_{CCN}.

3.6.2. Statistical characteristics and vertical variation in $f_{CCN/CN}$

$f_{CCN/CN}$ is the proportion of CCN to CN ($f_{CCN/CN}$ = CCN/CN) in this paper (Roberts et al., 2006). Aerosol size and chemical composition determine the capacity of aerosol particles to act as CCN (Frank et al., 2006). Many studies concerning the relationship of CN to CCN under different SS conditions have been made (Roberts et al., 2001, 2006; Yum and Hudson, 2001; Hudson and Yum, 2002; Andreae et al., 2004; Zhang et al., 2011). As more aerosol particles are activated into CCN with increasing SS, the $f_{CCN/CN}$ under the two SS setting (0.3% and 0.4%) was calculated using data from all flights. The maximum $f_{CCN/CN}$ was 0.92 with an average of 0.43 for SS = 0.4% and the maximum $f_{CCN/CN}$ was 0.74 with an average of 0.26 when SS = 0.3%. The mean value of $f_{CCN/CN}$ for SS = 0.4% is roughly twice that when SS = 0.3%. Also, the $f_{CCN/CN}$ on the hazy day was smaller than on the clear days, because the concentration of fine aerosols was large, which led to a relatively lower mean

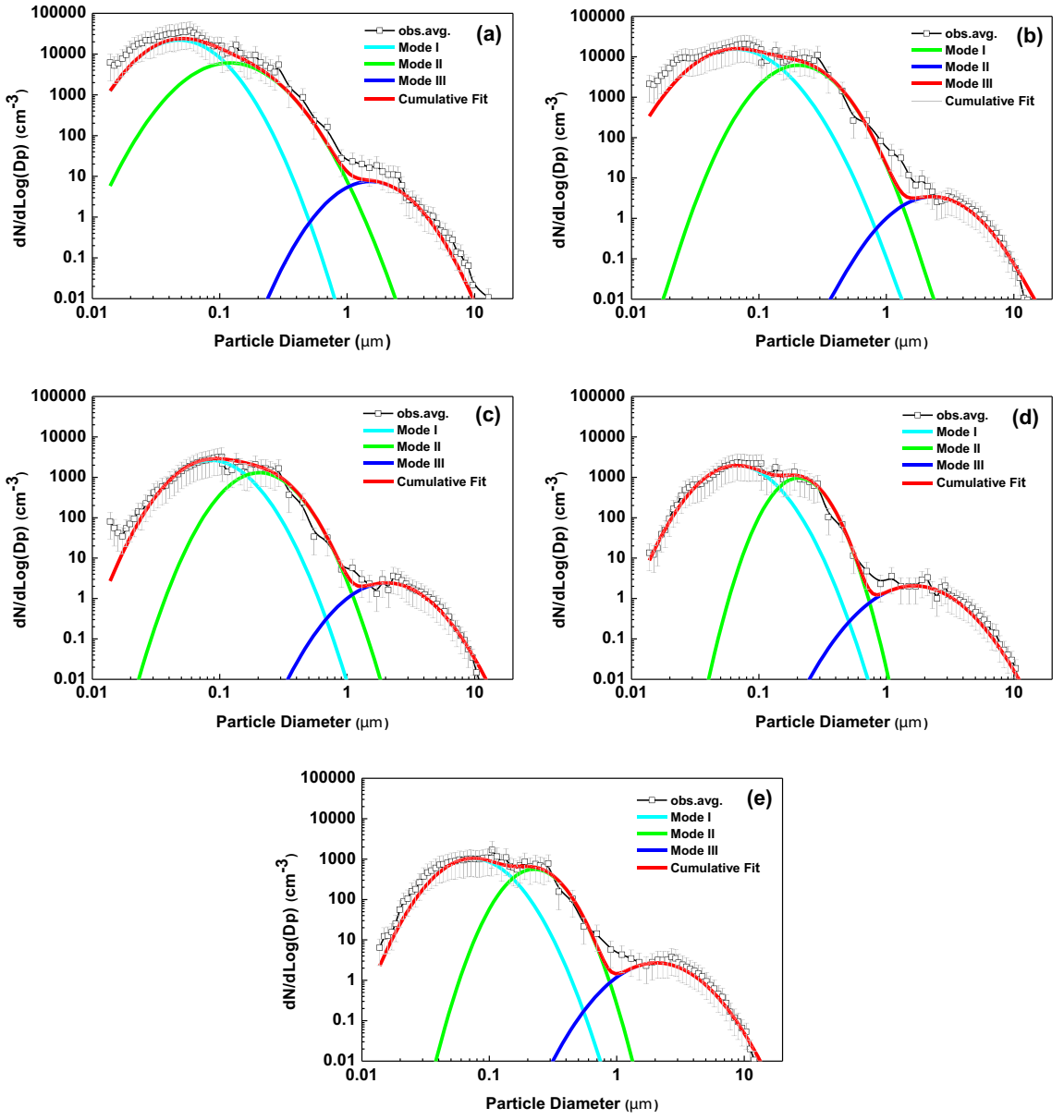

Fig. 6. Mean size distribution of aerosol particles from (a) 778–1000 m, (b) 1000–2000 m, (c) 2000–3000 m, (d) 3000–4000 m, and (e) 4000–5000 m. The line composed of black hollow squares represents the mean aerosol size distribution. Vertical gray lines show the error bars. The solid red line represents the cumulative fit of the total aerosol size distribution, and the cyan (Mode I — nucleation), green (Mode II — accumulation), and dark blue (Mode III — coarse) solid lines represent the lognormal fits of the three aerosol mode size distributions, respectively.

$f_{CCN/CN}$ on that day compared to later days. Size-resolved and bulk activation properties of aerosols were investigated over the North China Plain (Deng et al., 2011, 2013). That study found that the active ratio of accumulation mode aerosol particles was more than 0.6 at SS = 0.2% and more than 0.8 at SS = 0.4%. $f_{CCN/CN}$ values over the Loess Plateau presented in this study are less than those reported by Deng et al. (2011, 2013). Low values of $f_{CCN/CN}$ at the same SS levels in this study may illustrate that the proportion of fine aerosol particles measured during the flight campaign was higher and that these particles were not easily activated.

Average values of $f_{CCN/CN}$ at 100-m intervals from the surface to 4500 m and at 0.3% and 0.4% SS levels are shown in Fig. 9. The mean value of $f_{CCN/CN}$ has no obvious trend with altitude at SS = 0.3% (Fig. 9a), but the mean value of AR increases with altitude when SS = 0.4% (Fig. 9b). The vertical profile of $f_{CCN/CN}$, especially at the higher supersaturation (Fig. 9b), appears similar to the vertical profiles of ED (Fig. 5). A combination of three factors might explain the increase in $f_{CCN/CN}$ with altitude. First, the number concentration of aerosol particles is lower at higher altitude (Fig. 4). Second, ED increases with altitude and most of the large particles are distributed at higher altitudes (Fig. 5). Third, large particles are more likely to be CCN under higher SS conditions in most cases. Much research has been done with regard to the importance of the aerosol spectrum and chemical composition when

Table 4
Parameters characterizing the number size distributions of the three aerosol modes in different altitude zones. (N_a: cm^{-3}, D_g: μm).

Altitude ASL (m)	Mode I			Mode II			Mode III		
	N_a	D_g	logσ	N_a	D_g	logσ	N_a	D_g	logσ
778–1000	28,699	0.048	0.52	8816	0.122	0.58	7.8	1.45	0.52
1000–2000	21,750	0.065	0.56	7264	0.204	0.47	4.6	2.33	0.53
2000–3000	3248	0.084	0.49	1464	0.205	0.45	3.3	2.05	0.54
3000–4000	2364	0.067	0.48	823	0.205	0.34	3.0	1.65	0.58
4000–5000	1245	0.074	0.48	537	0.225	0.38	3.8	2.05	0.56

calculating CCN. Kuwata et al. (2008) showed that aerosol chemical composition is more important at lower SS than at higher SS. The ability of aerosol particles to be CCN is largely controlled by aerosol size rather than composition (Junge and McLaren, 1971; Fitzgerald, 1973). Dusek et al. (2006) also reported that the aerosol number size distribution determines the CCN concentration. Under the same SS conditions, large particles are more likely to be CCN, and small particles are not easily to be CCN, so $f_{CCN/CN}$ increases with increases in particle size. Zhang et al. (2011) studied the vertical distributions of N_a and aerosol effective radius (R_e), CCN, and $f_{CCN/CN}$ from aircraft measurements made over the Beijing region. The vertical profile of $f_{CCN/CN}$ was similar to the vertical profile of R_e in that paper, which is consistent with results presented here. This suggests that particle size is one of the crucial factors in the CCN fraction of aerosol particles.

4. Conclusions

The vertical profiles of aerosol particle number concentration and size distributions were obtained through analyses of aerosol measurements collected during a summertime aircraft campaign (31 July 2013 to 5 August 2013) over the Loess Plateau. The CCN activation properties of aerosols under different supersaturation conditions were also studied.

Mean nucleation and accumulation mode aerosol number concentrations were on the order of 10^3 cm^{-3}, with a maximum magnitude of 10^4 cm^{-3}. Thus, the majority of aerosols distributed over the China Loess Plateau during the summer of 2013 were mainly fine particles. The aerosol number concentration on one hazy day was two times greater than on cleaner days. Aerosol number concentrations decreased with altitude, with the first peak appearing between 1000 and 1400 m. A second peak appeared between 2000 and 3000 m. Vertical profiles of nucleation and accumulation mode aerosol number concentrations can be grossly fit with exponential functions. Aerosol particle diameters generally increased gradually with altitude. A rapid increase in aerosol

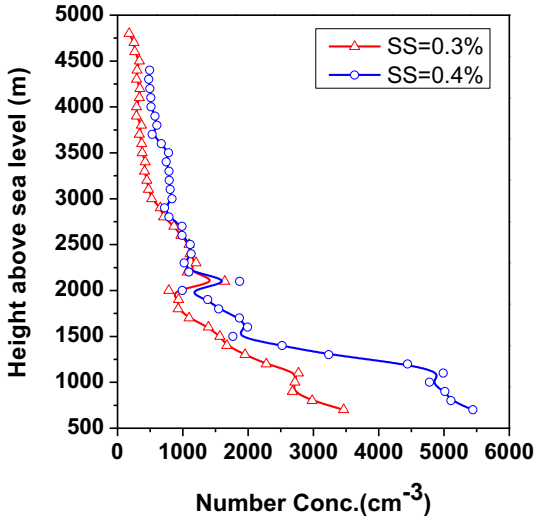

Fig. 7. Vertical distribution of average N_{CCN} at 0.3% and 0.4% SS measured on the flights.

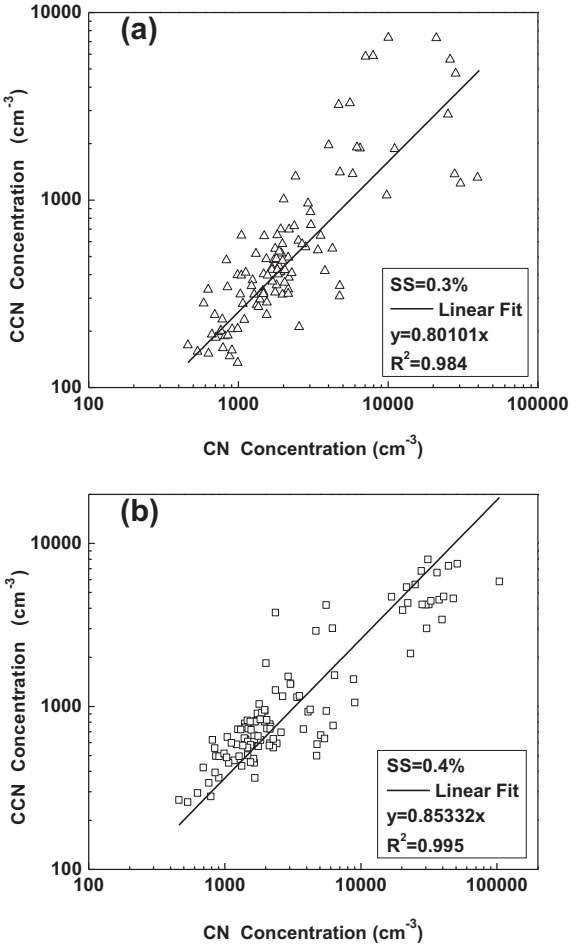

Fig. 8. CCN concentration as a function of CN concentration (a) at 0.3% and (b) 0.4% SS. Linear fits (black lines) to the data are shown.

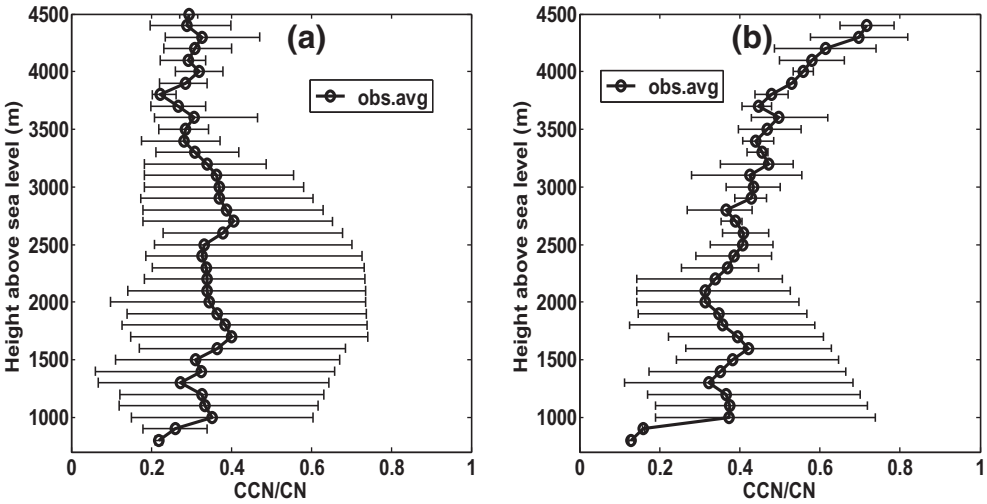

Fig. 9. Vertical profiles of mean $f_{CCN/CN}$ (a) at 0.3% and (b) 0.4% supersaturation (solid black lines with hollow circles). Horizontal black lines show the range of values (minimum and maximum values) observed at each altitude.

particle size was observed from 2000 to 2500 m. The presence of a temperature inversion layer is the main reason for the accumulation of aerosols near the surface. From the perspective of aerosol concentrations and vertical size distributions, fine particles at low altitudes contributed the most to the total aerosol concentration.

A sharp decrease in the aerosol number concentration is seen in the aerosol particle size distribution at 0.2 μm. From the ground to 5000 m, the total aerosol concentration decreased and the width of the aerosol spectral distribution narrows in nucleation and accumulation mode, but broadens slightly in coarse mode. Aerosol number size distributions in different height ranges showed two or three peaks. Tri-modal lognormal size distribution functions fit total aerosol number size distributions from 0.01 μm to 20 μm in each height range reasonably well.

N_{CCN} decreased with altitude. The relationship between N_{CCN} and N_a was analyzed and a closer linear relationship was found. $f_{CCN/CN}$ at supersaturation levels of 0.3% and 0.4% was analyzed. The $f_{CCN/CN}$ for SS = 0.3% was half of that when SS = 0.4%. The vertical profile of AR was similar to the vertical profile of ED, and the value of $f_{CCN/CN}$ increased with altitude.

Acknowledgments

The study is supported partially by the Ministry of Science and Technology of China under its national key project on global change studies (2013CB955804), the Special Fund for doctorate programs in Chinese Universities (Grant No. 20113228110002), the Public Meteorology Special Foundation of MOST (GYHY201306065) and (GYHY201206025), the Shanxi Meteorological Bureau key research projects (SXKZDTC20140605), and the Priority Academic Program of Development of Jiangsu Higher Education Institutions (PAPD).

References

Anderson, T.L., Masonis, S.J., Covert, D.S., Ahlquist, N.C., Howell, S.g., et al., 2003. Variability of aerosol optical properties derived from in situ aircraft measurements during ACE-Asia. J. Geophys. Res. 108 (D23), 8647. http://dx.doi.org/10.1029/2002JD003247.

Andreae, M.O., Rosenfeld, D., 2008. Aerosol–cloud–precipitation interactions. Part 1. The nature and sources of cloud-active aerosols. Earth Sci. Rev. 89, 13–41.

Andreae, M.O., et al., 2004. Smoking rain clouds over the Amazon. Science 303, 1337–1342.

Calvo, A.I., Alves, C., Castro, A., et al., 2013. Research on aerosol sources and chemical composition: past, current and emerging issues. Atmos. Res. 120–121, 1–28.

Campbell, James R., Reid, Jeffrey S., Westphal, Douglas L., et al., 2013. Characterizing the vertical profile of aerosol particle extinction and linear depolarization over Southeast Asia and the Maritime Continent: the 2007–2009 view from CALIOP. Atmos. Res. 122, 520–543.

Cui, Z., Carslaw, K.S., Yin, Y., Davies, S., 2006. A numerical study of aerosol effects on the dynamics and microphysics of a deep convective cloud in a continental environment. J. Geophys. Res. 111, D05201. http://dx.doi.org/10.1029/2005JD005981.

DeFelice, T.P., 1996. Variation in cloud condensation nuclei at palmer station Antarctica during February 1994. Atmos. Res. 41, 229–248.

DeFelice, T.P., Saxena, V.K., 1994. On the variation of cloud condensation nuclei in association with cloud systems at a mountain-top location. Atmos. Res. 31, 13–39.

Deng, Z.Z., Zhao, C.S., Ma, N., et al., 2011. Size-resolved and bulk activation properties of aerosols in the North China Plain. Atmos. Chem. Phys. 11, 3835–3846. http://dx.doi.org/10.5194/acp-11-3835-2011.

Deng, Z.Z., Zhao, C.S., Ma, N., et al., 2013. Examination of parameterizations for CCN number concentrations based on in-situ aerosol activation property measurements in the North China Plain. Atmos. Chem. Phys. Discuss. 13, 145–176. http://dx.doi.org/10.5194/acpd-13-145-2013 (www.atmos-chem-phys-discuss.net/13/145/2013/).

Dusek, U., Frank, G.P., Hildebrandt, L., et al., 2006. Size matters more than chemistry for cloud-nucleating ability of aerosol particles. Science 312, 1375–1378.

Fan, J., Leung, L.R., Li, Z., Morrison, H., Chen, H., Zhou, Y., Qian, Y., Wang, Y., 2012. Aerosol impacts on clouds and precipitation in eastern China: results from bin and bulk microphysics. J. Geophys. Res. 117, D00K36. http://dx.doi.org/10.1029/2011JD016537.

Fernández-Gálvez, J., et al., 2013. Aerosol size distribution from inversion of solar radiances and measured at ground-level during SPALI10 campaign. Atmos. Res. 127. http://dx.doi.org/10.1016/j.atmosres.2012.03.015.

Fitzgerald, J.W., 1973. Dependence of the supersaturation spectrum of CCN on aerosol size distribution and composition. J. Atmos. Sci. 30 (4), 628–634.

Frank, G.P., Dusek, U., Andreae, M.O., 2006. Technical note: a method for measuring size-resolved CCN in the atmosphere. Atmos. Chem. Phys. Discuss. 6 (3), 4879–4895.

Ghan, S.J., Collins, D.R., 2004. Use of in situ data to test a Raman lidar-based cloud condensation nuclei remote sensing method. J. Atmos. Ocean. Technol. 21, 387–394.

Ghan, S.J., Rissman, T.A., Elleman, R., Ferrare, R.A., Turner, D., Flynn, C., Wang, J., Ogren, J., Hudson, J., Jonsson, H.H., VanReken, T., Flagan, R.C., Seinfeld, J.H., 2006. Use of in situ cloud condensation nuclei, extinction and aerosol size distribution measurements to test a method for retrieving cloud condensation nuclei profiles from surface measurements. J. Geophys. Res. 111, D05S10. http://dx.doi.org/10.1029/2004JD005752.

Gras, J.L., 1995. CN, CCN and particle size in southern ocean air at Gape Grim. Atmos. Res. 35, 233–251.
Grützun, V., Knoth, O., Simmel, M., 2008. Simulation of the influence of aerosol particle characteristics on clouds and precipitation with LM-SPECS: model description and first results. Atmos. Res. 90, 233–242.
Han, Z., Montague, D.C., Snider, J.R., 2003. Airborne measurements of aerosol extinction in the lower and middle troposphere over Wyoming, USA. Atmos. Environ. 37, 789–802.
Han, Y., Fang, X., Zhao, T., Kang, S., 2008. Long range trans-Pacific transport and deposition of Asian dust aerosols. J. Environ. Sci. 20, 424–428.
Haywood, J.M., Boucher, O., 2000. Estimates of the direct and indirect radiative forcing due to tropospheric aerosols: a review. Rev. Geophys. 38, 513–543.
Haywood, J., Francis, P., Dubovik, O., Glew, M., Holben, B., 2003. Comparison of aerosol size distributions, radiative properties, and optical depths determined by aircraft observations and Sun photometers during SAFARI 2000. J. Geophys. Res. 108 (D13), 8471. http://dx.doi.org/10.1029/2002JD002250.
Hudson, J.G., Mishra, S., 2007. Relationships between CCN and cloud microphysics variations in clean maritime air. Geophys. Res. Lett. 34, L16804. http://dx.doi.org/10.1029/2007GL030044.
Hudson, J.G., Noble, S., 2009. CCN and cloud droplet concentrations at a remote ocean site. Geophys. Res. Lett. 36, L13812. http://dx.doi.org/10.1029/2009GL038465.
Hudson, J.G., Noble, S., 2014a. CCN and vertical velocity influences on droplet concentrations and supersaturations in clean and polluted stratus clouds. J. Atmos. Sci. 71, 312–331. http://dx.doi.org/10.1175/JAS-D-13-086.1.
Hudson, J.G., Noble, S., 2014b. Low altitude summer/winter microphysics, dynamics and CCN spectra of northeastern Caribbean small cumuli; and comparisons with stratus. J. Geophys. Res. Atmos. 119. http://dx.doi.org/10.1002/2013JD021442.
Hudson, J.G., Yum, S.S., 2001. Maritime-continental drizzle contrasts in small cumuli. J. Atmos. Sci. 58, 915–926.
Hudson, J.G., Yum, S.S., 2002. Cloud condensation nuclei spectra and polluted and clean clouds over the Indian Ocean. J. Geophys. Res. 107 (D19). http://dx.doi.org/10.1029/2001JD000829.
Hudson, J.G., Noble, S., Jha, V., Mishra, S., 2009. Correlations of small cumuli droplet and drizzle drop concentrations with cloud condensation nuclei concentrations. J. Geophys. Res. 114, D05201. http://dx.doi.org/10.1029/2008JD010581.
Hudson, J.G., Noble, S., Jha, V., 2010. Comparisons of CCN with supercooled clouds. J. Atmos. Sci. 67 (9), 3006–3018.
Hudson, J.G., Jha, V., Noble, S., 2011. Drizzle correlations with giant nuclei. Geophys. Res. Lett. 38, L05808. http://dx.doi.org/10.1029/2010GL046207.
Hudson, J.G., Noble, S., Jha, V., 2012. Cloud droplet spectral width relationship to CCN spectra and vertical velocity. J. Geophys. Res. 117, D11211. http://dx.doi.org/10.1029/2012JD017546.
IPCC, 2007. Climate Change 2007: The Physical Science Basis. Cambridge University Press, Cambridge, UK and New York, NY, USA (996 pp.).
Johnson, D.W., et al., 2000. Observations of the evolution of the aerosol, cloud and boundary-layer characteristics during the 1st ACE-2 Lagrangian experiment. Tellus 52B, 348–374.
Junge, C., McLaren, E., 1971. Relationship of cloud nuclei spectra to aerosol size distribution and composition. J. Atmos. Sci. 28, 382–390.
Kar, S.K., Liou, Y.A., Ha, K.J., 2009. Aerosol effects on the enhancement of cloud-to-ground lightning over major urban areas of South Korea. Atmos. Res. 92, 80–87.
Kuwata, M., Kondo, Y., Miyazaki, Y., et al., 2008. Cloud condensation nuclei activity at Jeju Island, Korea in spring 2005. Atmos. Chem. Phys. 8, 2933–2948.
Levin, Z., Teller, A., Ganor, E., Yin, Y., 2005. On the interactions of mineral dust, sea-salt particles, and clouds: a measurement and modeling study from the Mediterranean Israeli Dust Experiment campaign. J. Geophys. Res. 110, D20202. http://dx.doi.org/10.1029/2005JD005810.
Li, Z., Zhao, X., Kahn, R., Mishchenko, M., Remer, L., Lee, K.-H., Wang, M., Laszlo, I., Nakajima, T., Maring, H., 2009. Uncertainties in satellite remote sensing of aerosols and impact on monitoring its long-term trend: a review and perspective. Ann. Geophys. 27, 2755–2770.
Li, W., Li, P., Sun, G., Zhou, S., Yuan, Q., Wang, W., 2011a. Cloud residues and interstitial aerosols from non-precipitating clouds over an industrial and urban area in northern China. Atmos. Environ. 45, 2488–2495.
Li, Z., Li, C., Chen, H., et al., 2011b. East Asian Studies of Tropospheric Aerosols and their Impact on Regional Climate (EAST-AIRC): an overview. J. Geophys. Res. 116, D00K34. http://dx.doi.org/10.1029/2010JD015257.
Li, Z., Niu, F., Fan, J., Liu, Y., Rosenfeld, D., Ding, Y., 2011c. Long-term impacts of aerosols on the vertical development of clouds and precipitation. Nat. Geosci. 4, 888–894.
Li, W., Shi, Z., Zhang, D., Zhang, X., Li, P., Feng, Q., Yuan, Q., Wang, W., 2012. Haze particles over a coal-burning region in the China Loess Plateau in winter: three flight missions in December 2010. J. Geophys. Res. 117, D12306. http://dx.doi.org/10.1029/2012JD017720.
Li, Li, Dongjue, Dai, Shihuai, Deng, et al., 2013. Concentration, distribution and variation of polar organic aerosol tracers in Ya'an, a middle-sized city in western China. Atmos. Res. 120–121, 29–42.
Liu, P., Zhao, C., Zhang, Q., Deng, Z., Huang, M., Ma, X., Tie, X., 2009. Aircraft study of aerosol vertical distributions over Beijing and their optical properties. Tellus 61 (B), 756–767.
Liu, J., Zheng, Y., Li, Z., Cribb, M., 2011. Analysis of cloud condensation nuclei properties at a polluted site in southeastern China during the AMF-China Campaign. J. Geophys. Res. 116, D00K35. http://dx.doi.org/10.1029/2011jd016395.
Liu, J., Zheng, Y., Li, Z., Flynn, C., Cribb, M., 2012. Seasonal variations of aerosol optical properties, vertical distribution and associated radiative effects in the Yangtze Delta region of China. J. Geophys. Res. 117, D00K38. http://dx.doi.org/10.1029/2011jd016490, 2012.
Lohmann, U., Feichter, J., 2005. Global indirect aerosol effects: a review. Atmos. Chem. Phys. 5, 715–737.
Ma, Xiaoyan, Yu, Fangqun, 2014. Seasonal variability of aerosol vertical profiles over east US and west Europe: GEOS-Chem/APM simulation and comparison with CALIPSO observations. Atmos. Res. 140–141, 28–37.
O'Connor, T.C., Jennings, S.G., O'Dowd, C.D., 2008. Highlights of fifty years of atmospheric aerosol research at Mace Head. Atmos. Res. 90, 338–355.
Roberts, G.C., Andreae, M.O., Zhou, J., Artaxo, P., 2001. Cloud condensation nuclei in the Amazon Basin: "Marine" conditions over a continent? Geophys. Res. Lett. 28, 2807–2810.
Roberts, G., Mauger, G., Hadley, O., Ramanathan, V., 2006. North American and Asian aerosols over the eastern Pacific Ocean and their role in regulating cloud condensation nuclei. J. Geophys. Res. 111, D13205. http://dx.doi.org/10.1029/2005JD006661.
Rose, D., Gunthe, S.S., Mikhailov, E., Frank, G.P., Dusek, U., Andreae, M.O., Pöschl, U., 2008. Calibration and measurement uncertainties of a continuous-flow cloud condensation nuclei counter (DMT-CCNC): CCN activation of ammonium sulfate and sodium chloride aerosol particles in theory and experiment. Atmos. Chem. Phys. 8, 1153–1179. http://dx.doi.org/10.5194/acp-8-1153-2008.
Sabbah, I., Hasan, Fatma M., 2008. Remote sensing of aerosols over the Solar Village, Saudi Arabia. Atmos. Res. 90, 170–179.
Salinas, Santo V., Ning, Chew Boon, Jukka, Miettinen, et al., 2013. Physical and optical characteristics of the October 2010 haze event over Singapore: a photometric and lidar analysis. Atmos. Res. 122, 555–570.
Seinfeld, J.H., Pandis, S.N., 1997. Atmospheric Chemistry and Physics. John Wiley & Sons, Inc., New York, USA, pp. 444–445.
Snider, J.R., Guibert, S., Brenguier, J.L., 2000. Lack of closure between dry and wet aerosol measurements: results from ACE-2. AIP Conf. Proc. 534 (1), 627–631.
Stettler, M., von Hoyningen-Huene, W., 1996. On the relation between haze layer and air mass aerosol at an urban location-Case studies. Atmos. Res. 40, 1–18.
Sun, X., et al., 2013. Seasonal and vertical variations in aerosol distribution over Shijiazhuang, China. Atmos. Environ. 81, 245–252.
Tao, W.-K., Chen, J.-P., Li, Z., Wang, C., Zhang, C., 2012. Impact of aerosols on convective clouds and precipitation. Rev. Geophys. 50, RG2001. http://dx.doi.org/10.1029/2011RG000369.
Terry, Deshler, 2008. A review of global stratospheric aerosol: measurements, importance, life cycle, and local stratospheric aerosol. Atmos. Res. 90, 223–232.
Wang, Honglei, Zhu, Bin, Shen, Lijuan, An, Junlin, Yin, Yan, Kang, Hanqing, 2014. Number size distribution of aerosols at Mt. Huang and Nanjing in the Yangtze River Delta, China: effects of air masses and characteristics of new particle formation. Atmos. Res. 150, 42–56.
Welton, E.J., Voss, K.J., Quinn, P.K., Flatau, P.J., Markowicz, K., et al., 2002. Measurements of aerosol vertical profiles and optical properties during INDOEX 1999 using micropulse lidars. J. Geophys. Res. 107, 8019. http://dx.doi.org/10.1029/2000JD000038.
Whitby, K.T., 1978. The physical characteristics of sulfur aerosols. Atmos. Environ. 12. http://dx.doi.org/10.1016/0004-6981(78)90196-8.
Xu, Junwei, Tao, Jun, Zhang, Renjian, et al., 2012. Measurements of surface aerosol optical properties in winter of Shanghai. Atmos. Res. 109–110, 25–35.
Yin, Y., Levin, Z., Reisin, T.G., Tzivion, S., 2000. The effects of giant cloud condensation nuclei on the development of precipitation in convective clouds-a numerical study. Atmos. Res. 53, 91–116.
Yin, Y., Wurzler, S., Levin, Z., Reisin, T.G., 2002. Interactions of mineral dust particles and clouds: effects on precipitation and cloud optical properties. J. Geophys. Res. 107 (D23), 4724. http://dx.doi.org/10.1029/2001JD001544.
Yin, Y., Chen, C., Kui, C., et al., 2010. An observational study of the microphysical properties of atmospheric aerosol at Mt. Huang. Trans. Atmos. Sci 33 (2), 129–136.
Yum, S.S., Hudson, J.G., 2001. Vertical distributions of cloud condensation nuclei spectra over the springtime Arctic Ocean. J. Geophys. Res. 106 (D14), 15,045–15,052.

Yum, S.S., Hudson, J.G., 2002. Maritime/continental microphysical contrasts in stratus. Tellus 54B, 61–73.
Yum, S.S., Hudson, J.G., 2004. Wintertime/summertime contrasts of cloud condensation nuclei and cloud microphysics over the Southern Ocean. J. Geophys. Res. 109, D06204. http://dx.doi.org/10.1029/2003JD003864.
Zhang, Q., Zhao, C., Tie, X., Wei, Q., Huang, M., Li, G., Ying, Z., Li, C., 2006. Characterizations of aerosols over the Beijing region: a case study of aircraft measurements. Atmos. Environ. 40, 4513–4527.
Zhang, Q., Ma, X., Tie, X., et al., 2009. Vertical distributions of aerosols under different weather conditions: analysis of in-situ aircraft measurements in Beijing, China. Atmos. Environ. 43, 5526–5535.
Zhang, Q., Quan, J., Tie, X., Huang, M., Ma, X., 2011. Impact of aerosol particles on cloud formation: aircraft measurements in China. Atmos. Environ. 45, 665–672.
Zhao, P., Yin, Y., Xiao, H., 2015. The effects of aerosol on development of thunderstorm electrification: a numerical study. Atmos. Res. 153, 376–391.